THE JOURNAL OF PHYSICAL CHEMISTRY Letters

Letter

pubs.acs.org/JPCL

Interstitial Lithium Diffusion Pathways in γ-$LiAlO_2$: A Computational Study

Mazharul M. Islam* and Thomas Bredow

Mulliken Center for Theoretical Chemistry, Institut für Physikalische und Theoretische Chemie, University of Bonn, Beringstrasse 4-6, D-53115 Bonn, Germany

Supporting Information

ABSTRACT: Although the Li diffusion in single crystalline γ-$LiAlO_2$ was studied with temperature-dependent Li-7 NMR spectroscopy and conductivity measurements recently, the exact diffusion pathways are not yet clearly identified. Therefore, the present study aims at elucidating the diffusion pathways in γ-$LiAlO_2$ theoretically from first principles. Competing pathways for Li diffusion are investigated using the climbing-image nudged-elastic-band approach with periodic quantum-chemical density functional theory (DFT) method. Li can migrate between two regular LiO_4 tetrahedral sites via Li point defect (V_{Li}) and via a Li Frenkel defect (V_{Li} + Li_i). On the basis of calculated activation energies for Li diffusion pathways, it is concluded that Li conductivity is strongly dependent on the distribution of Li vacancies and interstitial Li in the lattice. For Frenkel defects where Li_i is far away from the migrating Li atom, the calculated activation energies for jumps to nearest-neighbor vacant sites agree with experimental values.

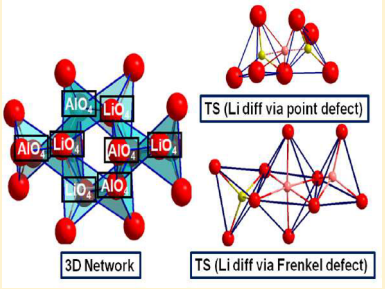

In recent years, γ-$LiAlO_2$ has attracted considerable attention due to its practical application as a coating in Li electrodes,[1,2] as an additive in composite Li electrolytes,[3] as a substrate material for epitaxial growth of III−V semiconductors like GaN,[4] and as a candidate material for tritium breeders or fusion reactors.[5,6] In all these applications, Li ion diffusion is a crucial process.

γ-$LiAlO_2$ crystallizes in the tetragonal space group $P4_12_12$ with lattice parameters a = 5.1687 ± 0.0005 Å and c = 6.2679 ± 0.0006 Å.[7] The unit cell contains four formula units (see Figure 1a). Both Li and Al atoms are located in oxygen tetrahedra where each LiO_4 tetrahedron shares a common edge with an AlO_4 tetrahedron. These pairs of LiO_4−AlO_4 tetrahedra are connected via common oxygen corners (see Figure 1b) and form a three-dimensional network with channels as shown in Figure 1c.

Li diffusion processes in γ-$LiAlO_2$ have been the subject of research interest for various recent experimental[8−11] and theoretical[12] studies. In a study of Li ion conductivity by impedance spectroscopy with increasing temperature,[8] it was observed that extrinsic conductivity occurs at temperatures of 200 °C due to Li ion diffusion. Indris et al.[9] studied the dynamics of lithium ions with temperature-dependent Li-7 NMR spectroscopy and conductivity measurements. They measured activation energies of Li ion diffusion between 0.70 and 1.26 eV, respectively. A temperature-dependent vibrational spectroscopic study[10] suggests that, on heating, the Li−O bonds break, and the Li ions could jump from one regular tetrahedral site to the next tetrahedral site with activation energies of 0.5−0.8 eV. A recent experimental study by temperature-dependent conductivity spectroscopy[11] revealed an increase of the room-temperature ionic conductivity in γ-$LiAlO_2$ due to the introduction of structural disorder caused by point defects or higher-dimensional defects. The measured activation energy for Li ion conduction ranges between 0.79 eV (for nanocrystalline/amorphous) and 1.13 eV (microcrystalline source material).[11] Classical molecular dynamics simulations predicted a Li diffusion coefficient of 2.8×10^{-11} m^2/s at 600 K and an activation energy of 0.5 eV.[12]

However, details of the Li diffusion pathway are not clearly described in any of these studies.

In the present study, a theoretical investigation of various possible migration pathways and activation barriers in γ-$LiAlO_2$ is performed using the first-principles density functional theory (DFT) method and periodic supercell models.

The Perdew−Burke−Ernzerhof (PBE) functional,[13,14] based on the generalized gradient approximation (GGA), was used as implemented in the plane-wave program VASP.[15,16] The projector-augmented wave (PAW) method was used for the core−electron representation.[17,18] We used a value of E_{cut} = 400 eV for the plane-wave expansion in the present study. Convergence tests employing larger E_{cut} (520, 600, and 800 eV) show that the lattice parameters (a and c) change by less than 0.03 Å, and the total energy has converged within 0.01 eV with E_{cut} = 400 eV. The integration in reciprocal space was performed with a 4 × 4 × 4 Monkhorst−Pack grid.[19] An energy convergence of 10^{-6} eV per cell was obtained with these values. The defective structures were simulated using $Li_4Al_4O_8$, $Li_{32}Al_{32}O_{64}$ and $Li_{108}Al_{108}O_{216}$ supercells with 4 × 4 × 4, 2 × 2 × 2 and 1 × 1 × 1 Monkhorst−Pack grid. The transition-state search for the migration processes was conducted with the

Received: August 13, 2015
Accepted: November 6, 2015
Published: November 6, 2015

DOI: 10.1021/acs.jpclett.5b01780
J. Phys. Chem. Lett. 2015, 6, 4622−4626

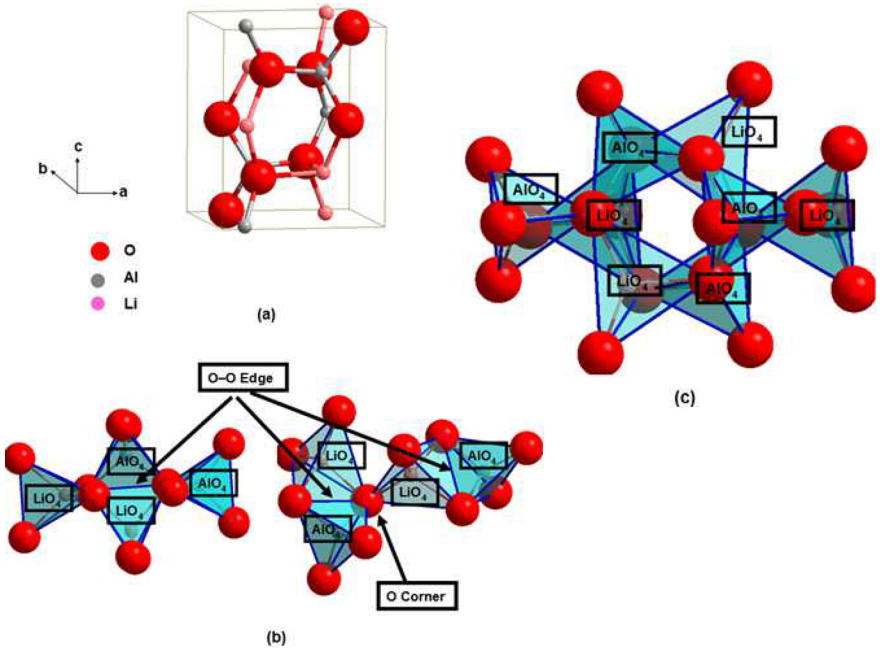

Figure 1. (a) Unit cell of γ-$LiAlO_2$. (b) Local structures showing the LiO_4 and AlO_4 tetrahedra shared by O-edge and LiO_4–AlO_4 pairs shared by O corners. (c) Formation of 3D channel by corners sharing of LiO_4–AlO_4 pairs.

climbing-image nudged-elastic-band (cNEB) method[20] as implemented in VASP. Vibrational-analysis calculations were performed to verify the true local-minimum or saddle-point character of the optimized geometries.

Prior to the study of ion diffusion in γ-$LiAlO_2$, the structural properties such as lattice parameters (a and c), bond lengths, and bond angles are calculated from a fully optimized system. The calculated lattice parameters are in reasonable agreement with experiment.[7] The maximum deviation is observed for c, −0.02 Å (corresponding to −0.5%; see Table 1). Also the calculated fractional coordinates for γ-$LiAlO_2$ are close to the experimental values[7] (Table 2). Our calculated tetrahedral Al–O and Li–O distances are 1.77 and 1.98 Å, which are in good agreement with the experimental bond distances of 1.765 and 2.00 Å, respectively.[7] The deviation is less than 0.05 Å (see Table 1). The LiO_4 tetrahedron (with Li–O distances 2.05 Å (2×), 1.93 Å(2×)) is more distorted than AlO_4 (with Al–O distances ranging from 1.76 to 1.77 Å). The shared edge between the LiO_4 and AlO_4 tetrahedra has a length of 2.73 Å, which is significantly shorter than the average distance of the other edges of LiO_4 (3.34 Å) and AlO_4 (2.91 Å).

To the best of our knowledge, the exact diffusion pathway for Li ion diffusion in γ-$LiAlO_2$ is not yet identified. In the present study, we have investigated various diffusion processes in γ-$LiAlO_2$ in order to elucidate the local diffusion mechanisms. Test calculations employing $Li_4Al_4O_8$, $Li_{32}Al_{32}O_{64}$, and $Li_{108}Al_{108}O_{216}$ supercells show that diffusion properties are converged with a medium-sized supercell ($Li_{32}Al_{32}O_{64}$). Therefore, this supercell was used for Li ion diffusion in γ-$LiAlO_2$.

As depicted in Figure 2a, Li can migrate from its regular LiO_4 tetrahedral location to the nearest empty tetrahedral site (1-NN) after formation of a Li point defect, V_{Li} (the yellow atom in the first figure of Figure 2a). In this case, the migrating Li atom passes through the channel via a LiO_4 tetrahedral site in the transition state (Figure 2a). In the transition state structure, two of the four Li–O distances are larger (2.51 and 2.60 Å), and the other two (1.80 and 1.88 Å) are shorter than the average Li–O distance (2.0 Å) of a regular LiO_4 tetrahedron. Our calculated activation energy for this 1-NN migration process is 0.65 eV (see Table 3), which is in the lower range of experimental values. The effect of E_{cut} on the calculated activation energy was explicitly tested by a recalculation of the 1-NN migration process at E_{cut} = 520 eV. In this way the

Table 1. Comparison of Calculated Lattice Parameters (Å), Bond Distances (Å), and Bond Angles (Degrees) with Available Experimental Data[7]

lattice parameters	calc.	exp.
a	5.152	5.1687
c	6.240	6.2679
bond distances AlO_4		
Al–O (2)	1.760	1.755
Al–O (2)	1.774	1.766
O–O(2)	2.920	2.918
O–O(2)	2.910	2.896
O–O	2.890	2.874
O–O	2.734	2.737
bond distances LiO_4		
Li–O(2)	2.035	2.059
Li–O(2)	1.923	1.948
O–O(2)	3.370	3.301
O–O(2)	3.290	3.296
O–O	3.400	3.430
O–O	2.734	2.737
Al–Al	3.109	3.118
Li–Li	3.081	3.091
Al–Li	2.637	2.656
bond angles		
O–Al–O	110.9	110.7
O–Li–O	110.7	110.6
Al–O–Li	115.8	115.6
Al–O–Al	124.3	124.6
Li–O–Li	100.8	100.9

DOI: 10.1021/acs.jpclett.5b01780
J. Phys. Chem. Lett. 2015, 6, 4622–4626

Table 2. Comparison of Calculated Atomic Coordinates with Available Experimental Data[7]

	x		*y*		*z*	
atoms	calc.	exp.	calc.	exp.	calc.	exp.
O	0.3332	0.3369	0.2929	0.2906	0.7695	0.7723
Al	0.1752	0.1759	0.1752	0.1759	0.0	0.0
Li	0.8132	0.8126	0.8132	0.8126	0.0	0.0

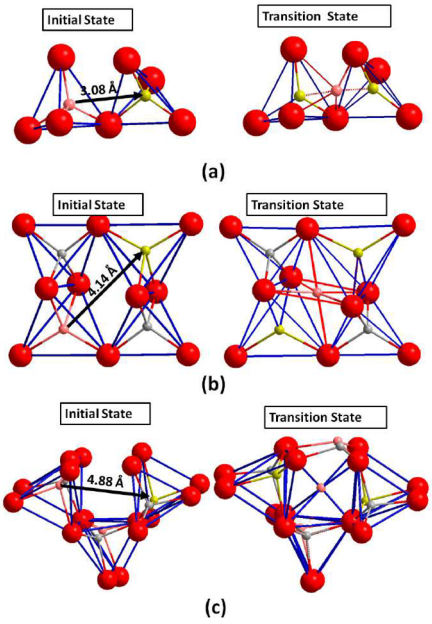

Figure 2. Li migration pathway via point defect for a Li jump from a regular tetrahedral site to the first nearest tetrahedral location (a), to the second nearest tetrahedral location (b), and to the third nearest tetrahedral location (c). The red, pink and yellow disks represent oxygen atoms, lithium atoms, and lithium vacancies, respectively.

Table 3. Calculated Activation Energy E_A for Li Diffusion in γ-$LiAlO_2$ Containing a Li Point Defect

d_{Li-Li} (Å)	E_A (eV)
3.08	0.65
4.14	1.65
4.88	1.41

calculated activation energy is 0.63 eV, which is only 0.02 eV smaller than that obtained with E_{cut} = 400 eV. We therefore conclude that the computational accuracy parameters are well converged.

The point defect migration was considered for a Li jump from its regular LiO_4 tetrahedral location to the second and third nearest (2-NN and 3-NN) tetrahedral sites as shown in Figure 2b,c, respectively. In both cases, Li migrates through a distorted octahedral interstitial site. The calculated activation energies for this pathway are much larger than for a 1-NN jump, 1.65 and 1.41 eV, respectively (Table 3). The average Li−O distance of the distorted LiO_6 octahedron is shorter in Li migration to 2-NN Li vacancy than that in 3-NN Li vacancy (Figure 2b,c). This may lead to a stronger repulsion and therefore may be responsible for the slightly larger activation energy.

Li can jump from its regular LiO_4 tetrahedral location to the 3-NN nearest LiO_4 tetrahedral sites (4.88 Å) through the large channel via a Li Frenkel defect, V_{Li} + Li_i (as shown in Figure 3).

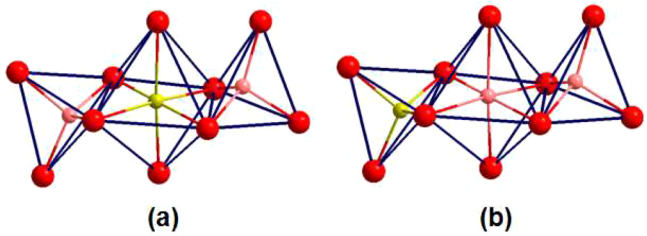

Figure 3. Li migration pathway for a Li jump from a regular tetrahedral site to the third nearest tetrahedral location via the Li Frenkel defect, through the channel via an octahedral interstitial site: (a) initial structure and (b) transition state. The red, pink and yellow disks represent oxygen atoms, lithium atoms, and lithium vacancies, respectively.

The migration pathway consists of two hopping processes: first a Li migration from the regular site to the V_{Li} at Frenkel position (yellow atom in Figure 3a) and second a Li migration from the Frenkel position to the nearest regular LiO_4 location (as shown in Figure 3b). The activation energy for this hopping process is 1.78 eV, which is higher than the Li migration via point defect to the 3-NN Li position (1.41 eV). This is probably due to the electrostatic repulsion between the migrating Li (Li_{Mig}) and the interstitial Li (Li_i), which is not present in the diffusion mechanisms involving Li vacancies. In order to verify this hypothesis, we studied the above-mentioned three migration pathways (1-NN, 2-NN, 3-NN) with a Frenkel defect instead of V_{Li} by varying the position of Li_i. For 1-NN Li migration (d_{Li-Li} = 3.08 Å), three new migration pathways were studied where Li_{Mig}−Li_i distances are 1.88, 3.63, and 6.52 Å, respectively. The formation energies of these Frenkel defects are within 0.1 eV, indicating that the interaction between V_{Li} and Li_i is small. This means that, in principle, all V_{Li}−Li_i distances may exist at ambient conditions, and all three pathways have a similar probability. The calculated activation energies for the three pathways are 0.93, 0.68, and 0.64 eV, respectively (see Table 4). This confirms the assumption of the effect of Li−Li repulsion in the transition structure on the activation energy.

Table 4. Calculated Activation Energy E_A (eV) for Li Diffusion in γ-$LiAlO_2$ Containing a Frenkel Defect in Dependence of the Distance between Li_i and the Migrating Li $d_{Li_{Mig}-Li_i}$ (Å)

d_{Li-Li}	$d_{Li_{Mig}-Li_i}$	E_A
3.08	1.88	0.93
	3.63	0.68
	6.52	0.64
4.14	2.07	1.21
	2.43	1.17
	5.04	1.71
4.88	2.44	1.78
	3.67	1.52
	6.51	1.45

Similarly, for the 2-NN Li diffusion (d_{Li-Li} = 4.14 Å), the three investigated migration pathways have Li_{Mig}−Li_i distances of 2.07, 2.43, and 5.04 Å. The corresponding activation energies are 1.21, 1.17, and 1.71 eV, respectively (see Table 4). Here it is surprising that the largest Li_{Mig}−Li_i distance leads to a larger barrier.

DOI: 10.1021/acs.jpclett.5b01780
J. Phys. Chem. Lett. 2015, 6, 4622−4626

Finally, for the 3-NN Li diffusion (d_{Li-Li} = 4.88 Å), the migration pathways are characterized by Li_{Mig}–Li_i distances 2.44, 3.67, and 6.51 Å. The activation energies are 1.78, 1.52, and 1.45 eV, respectively (see Table 4).

These findings reveal that there is substantial repulsive interaction between the migrating Li and the interstitial Li when they are in a close distance, which in turn increases the activation barrier, at least for the 1-NN and 3-NN migration pathways. In order to clarify the opposite trend observed for the third structure of the 2-NN pathway, we have analyzed three transition state structures (TS) for the 2-NN migration pathways. In all cases, the TS corresponds to a distorted LiO_6 octahedron. For the migration pathways with smaller Li_{Mig}–Li_i distance (2.07 and 2.43 Å), four Li–O distances are less than 2.0 Å, and the remaining two Li–O bonds are in the range of 2.6 to 2.8 Å. On the other hand, for the Li migration in the case of the largest Li_{Mig}–Li_i distance (5.04 Å), all the Li–O bonds are in the range of 2.0–2.2 Å. Therefore, we assume that Li migration in this pathway faces more hindrance from Li–O interaction than the former cases, which makes the activation energy larger.

In any case, at very large Li_{Mig}–Li_i distances, the activation energy converges to the values obtained for the migration via Li point defect. This suggests that in the limit of infinite V_{Li}–Li_i or Li_{Mig}–Li_i distance, both mechanisms are indistinguishable.

From the calculated activation barriers it follows that, although Li vacancies are essential for Li conductivity of γ-$LiAlO_2$, the most likely Li migration process may involve Frenkel defects. For this defect type it is observed that the activation barrier of local Li ion jumps is a function of the V_{Li}–Li_i and Li_{Mig}–Li_i distances. This can explain the relatively large scatter of the experimental values.

In summary, we have investigated the structure, possible migration pathways, and activation barriers in γ-$LiAlO_2$ using the first-principles DFT method and periodic supercell models. The calculated activation energies for the migration with Li vacancy are 0.65 eV (1-NN), 1.65 eV (2-NN), and 1.41 eV (3-NN). The presence of an interstitial Li far from the migrating Li and Li vacancy leads to variations of the activation energy, namely from 0.64 to 0.93 eV for 1-NN, from 1.17 to 1.71 eV for 2-NN, and from 1.45 to 1.78 eV for 3-NN. It is important to note that in both type of migration pathways (via Li vacancy with or without the presence of interstitial Li) we have considered neutral supercells. By employing charged supercells with compensating homogeneous background charge for the 1-NN Li diffusion pathways, we obtained an activation energy of 0.60 eV, which is only 0.04 eV smaller than the smallest barrier obtained with neutral models. Therefore, for larger supercells, the difference between the two model types is expected to vanish.

The calculated activation energies of the 1-NN migration, and the smallest 2-NN activation energies are in the range of the measured values (0.70 to 1.26 eV[9] and 0.79 to 1.13 eV[11]). In general, GGA-DFT approaches underestimate experimental activation energies, as it was observed in the case of Li diffusion in Li_2O,[21] Li_2O:B_2O_3,[22] α-Li_3VF_6,[23] and $LiTiS_2$.[24] Accordingly, our calculated smallest activation energy (0.64 eV) is smaller than the smallest experimental value of 0.7 eV. Therefore, in the present case, the discrepancy is less pronounced.

Due to the rather similar Frenkel defect formation energies with variations of the V_{Li}–Li_i, a statistical distribution can be assumed. It is therefore concluded that the average V_{Li}–Li_i distance in Frenkel defects is large in real samples of γ-$LiAlO_2$.

■ ASSOCIATED CONTENT

Supporting Information

The Supporting Information is available free of charge on the ACS Publications website at DOI: 10.1021/acs.jpclett.5b01780.

Local structures showing the images of the 1-NN migration pathway in Figure S1 (PDF)

■ AUTHOR INFORMATION

Corresponding Author

*E-mail: rana-islam@thch.uni-bonn.de. Phone: +49 (0)228-732254. Fax: +49-(0)228-739064.

Notes

The authors declare no competing financial interest.

■ ACKNOWLEDGMENTS

M.M.I. is grateful to Deutsche Forschungsgemeinschaft (DFG) for the postdoctorate funding within DFG-Forschergruppe 1277 molife *Mobilität von Li-Ionen in Festkörpern.*

■ REFERENCES

(1) Ceder, G.; Chiang, Y. M.; Sadoway, D. R.; Aydinol, M. K.; Jang, Y. I.; Huang, B. Identification of cathode materials for lithium batteries guided by first-principles calculations. *Nature* **1998**, *392*, 694–696.

(2) Cao, H.; Xia, B.; Zhang, Y.; Xu, N. $LiAlO_2$-coated $LiCoO_2$ as cathode material for lithium ion batteries. *Solid State Ionics* **2005**, *176*, 911–915.

(3) Lakshman Dissanayake, M. A. K. Nano-composite solid polymer electrolytes for solid state ionic devices. *Ionics* **2004**, *10*, 221–225.

(4) Waltereit, P.; Brandt, O.; Trampert, A.; Grahn, H.; Menniger, J.; et al. Nitride semiconductors free of electrostatic fields for efficient white light-emitting diodes. *Nature* **2000**, *406*, 865–868.

(5) Botter, F.; Lefevre, F.; Rasneur, B.; Trotabas, M.; Roth, E. Effects of Radiation on Lithium Aluminate Samples Properties. *J. Nucl. Mater.* **1986**, *141*, 364–368.

(6) Arons, R.; Poeppel, R.; Tetenbaum, M.; Johnson, C. Preparation, Characterization, and Chemistry of Solid Ceramic Breeder Materials. *J. Nucl. Mater.* **1981**, *103*, 573–577.

(7) Marezio, M. The crystal structure and anomalous dispersion of γ-$LiAlO_2$. *Acta Crystallogr.* **1965**, *19*, 396–400.

(8) Alessandrini, F.; Alvani, C.; Casadio, S.; Mancini, M.; Nannetti, C. In-situ tritium release (CORELLI-2 experiment) and ex-reactor ionic conductivity of substoichiometric $LiAlO_2$ breeder ceramics. *J. Nucl. Mater.* **1995**, *224*, 236–244.

(9) Indris, S.; Heitjans, P.; Uecker, R.; Roling, B. Li Ion Dynamics in a $LiAlO_2$ Single Crystal Studied by ^{7}Li NMR Spectroscopy and Conductivity Measurements. *J. Phys. Chem. C* **2012**, *116*, 14243–14247.

(10) Hu, Q.; Lei, L.; Jiang, X.; Feng, Z. C.; Tang, M.; He, D. Li ion diffusion in $LiAlO_2$ investigated by Raman spectroscopy. *Solid State Sci.* **2014**, *37*, 103–107.

(11) Wohlmuth, D.; Epp, V.; Bottke, P.; Hanzu, I.; Bitschnau, B.; Letofsky-Papst, I.; Kriechbaum, M.; Amenitsch, H.; Hofer, F.; Wilkening, M. Order vs. disorder-a huge increase in ionic conductivity of nanocrystalline $LiAlO_2$ embedded in an amorphous-like matrix of lithium aluminate. *J. Mater. Chem. A* **2014**, *2*, 20295–20306.

(12) Jacobs, J.-P.; San Miguel, M. A.; Alvarez, L. J.; Giral, P. B. Lithium diffusion in γ-$LiAlO_2$, a molecular dynamics simulation. *J. Nucl. Mater.* **1996**, *232*, 131–137.

(13) Perdew, J.; Burke, K.; Ernzerhof, M. Generalized Gradient Approximation Made Simple. *Phys. Rev. Lett.* **1996**, *77*, 3865–3868.

(14) Perdew, J.; Burke, K.; Ernzerhof, M. Generalized Gradient Approximation Made Simple [Erratum Phys. Rev. Lett. 77, 3865 (1996)]. *Phys. Rev. Lett.* **1997**, *78*, 1396–1396.

(15) Kresse, G.; Hafner, J. Ab initio molecular dynamics for liquid metals. *Phys. Rev. B: Condens. Matter Mater. Phys.* **1993**, *47*, 558–561.

DOI: 10.1021/acs.jpclett.5b01780
J. Phys. Chem. Lett. 2015, 6, 4622–4626

(16) Kresse, G.; Hafner, J. Ab initio molecular-dynamics simulation of the liquid-metal-amorphous-semiconductor transition in germanium. *Phys. Rev. B: Condens. Matter Mater. Phys.* **1994**, *49*, 14251−14269.
(17) Kresse, G.; Joubert, D. From ultrasoft pseudopotentials to the projector augmented-wave method. *Phys. Rev. B: Condens. Matter Mater. Phys.* **1999**, *59*, 1758−1775.
(18) Blöchl, P. E. Projector augmented-wave method. *Phys. Rev. B: Condens. Matter Mater. Phys.* **1994**, *50*, 17953−17979.
(19) Monkhorst, H. J.; Pack, J. D. Special points for Brillouin-zone integrations. *Phys. Rev. B* **1976**, *13*, 5188−5192.
(20) Jonsson, H.; Mills, G.; Jacobsen, K. W. In *Classical and Quantum Dynamics in Condensed Phase Simulations*; Berne, B. J., Ciccotti, G., Coker, D. F., Eds.; World Scientific: Singapore, 1998; p 385.
(21) Islam, M. M.; Bredow, T.; Minot, C. Theoretical Analysis of Structural, Energetic, Electronic, and Defect Properties of Li_2O. *J. Phys. Chem. B* **2006**, *110*, 9413−9420.
(22) Islam, M. M.; Bredow, T.; Heitjans, P. The ionic conductivity in lithium-boron oxide materials and its relation to structural, electronic and defect properties: insights from theory. *J. Phys.: Condens. Matter* **2012**, *24*, 203201.
(23) Islam, M. M.; Wilkening, M.; Heitjans, P.; Bredow, T. Insights into Li^+ Migration Pathways in α-Li_3VF_6: A First-Principles Investigation. *J. Phys. Chem. Lett.* **2012**, *3*, 3120−3124.
(24) Wiedemann, D.; Islam, M. M.; Nakhal, S.; Senyshyn, A.; Bredow, T.; Lerch, M. Lithium Diffusion Pathways in 3R-Li_xTiS_2: A Combined Neutron Diffraction and Computational Study. *J. Phys. Chem. C* **2015**, *119*, 11370−11381.

DOI: 10.1021/acs.jpclett.5b01780
J. Phys. Chem. Lett. 2015, 6, 4622−4626